Age and growth of *Astarte borealis* (Bivalvia) from the southwestern Baltic Sea using Secondary Ion Mass Spectrometry

David K. Moss[1*], Donna Surge[2], Michael L. Zettler[3], Ian J. Orland[4,5], Alex Burnette[2], Abby Fancher[2]

Address info:

1. Department of Environmental and Geosciences, Sam Houston State University, Huntsville, TX 77431.

2. Department of Geological Sciences, University of North Carolina, Chapel Hill, NC 27599

3. Leibniz-Institute for Baltic Sea Research, Rostock, Germany

4. WiscSIMS, Department of Geoscience, University of Wisconsin-Madison, Madison, WI

5. Wisconsin Geological and Natural History Survye, University of Wisconsin-Madison, Madison, WI

*Corresponding author; dxm112@shsu.edu

Abstract

Traditional isotope sclerochronology employing isotope ratio mass spectrometry (IRMS) has been used for decades to determine the periodicity of growth increment formation in marine organisms with accretionary growth. Despite its well demonstrated capabilities, it is not without limitation. The most significant of these being the volume of carbonate powder required for analysis and convention drill-sampling techniques, which limit sampling to early in ontogeny when growth is fast or to species that reach relatively large sizes. In species like *Astarte borealis*

(Schumacher, 1817), a common component of Arctic boreal seas, traditional methods of increment analysis are difficult because the species is typically long lived, slow growing, and forms extremely narrowly spaced growth increments. Here we use Secondary Ion Mass Spectrometry (SIMS) to analyze $\delta^{18}O$ in 10-μm diameter spots and resolve the seasonal timing of growth increment formation in *Astarte borealis* in the southeastern Baltic Sea. In the individaul sampled here, dark growth increments can form in either the fall, winter, or spring. Futhermore, growth increment data from two populations (RFP3S = 54.7967°N, 12.38787°E; WA = 54.86775°N, 14.09832°E) indicate that in the Baltic Sea *A. borealis* is moderately long-lived (at least 43 years) and slow growing (von Bertalanffy k values 0.08 and 0.06). Our results demonstrate the potential of *A. borealis* to be a recorder of Baltic Sea seasonality over the past century using both live- and dead-collected shells, and also the ability of SIMS analysis to broaden the spectrum of bivalves used in sclerocrhonological work.

Declarations

Funding:

Conflicts of interest/competing interests: The authors are not aware of any conflicts of interest which may arise as a result of this work.

Availability of data and material: The datasets generated during and/or analysed during the current study will be made available in the Center for Open Science repository (http//osf.io).

Code availablility: Not applicable

Introduction

Isotope sclerochronlogy can be useful in determining the lifespan and growth history of marine organisms with accretionary hard parts. Organisms like bivalves, corals, and fish record their age-at-size in the form of growth increments, similar to the growth rings in trees. In bivalves, growth increments form in response to environmental and biological conditions and at several periodicities: daily, tidal, fortnightly, monthly, and annual (Barker 1964; Pannella and MacClintock 1968; Clark 1974; Pannella 1976; Jones et al. 1983; Goodwin et al. 2001). One method to determine the timing of these increments is to examine patterns in the variation of oxygen isotope ratios ($^{18}O/^{16}O$; $\delta^{18}O$ values) along the axis of maximum growth of the biogenic carbonate. Oxygen isotope ratios are, in part, a function of temperature and can show patterns reflecting seasonal variation, which can then be used to distinguish annual from non-annual growth increments (e.g., Jones and Quitmyer 1996; Schöne and Surge 2012). Identification of annual growth increments allows for an understanding of lifespan and growth rate.

Traditional methods of isotope sclerochronology employ a micromilling system fit with a silica carbide dental bit or tungsten carbide dental scriber point to extract carbonate powder for analysis via isotope ratio mass spectrometry (IRMS). Using a computerized system, the user is able to sample digitized paths of shell material perpendicular to growth increments in cross-sections. Growth is fastest early in ontogeny so sampling is typically focused on the youngest parts of shells to maximize the amount of carbonate powder drilled and to minimize time averaging. Except for techniques like incremental step drilling (e.g., Schöne et al. 2005a), where samples are only taken at the leading edge of the trench, it is often difficult to sample growth increments late in ontogeny as they are narrowly spaced and may exceed the width of the drill bit itself. In fast growing and/or large species, like *Mercenaria mercenaria* and *Arctica islandica*,

81 this is typically not a problem (e.g., Weidman et al. 1994; Quitmyer et al. 1997; Surge and
82 Walker 2006; Surge et al. 2007; Schöne 2013) but it can become an issue in small, slow growing,
83 long-livedspecies, like those from the genus *Astarte*.
84 Our previous work used traditional micromilling techniques to identify annual growth
85 increments in the shells of *Astarte borealis* (Schumacher, 1817) from the White Sea, Russia,
86 where individuals reach 35.5 mm in length (Moss et al. 2018). There, individuals grow relatively
87 slowly, experience growth slow-downs in the summer months that result in annual increment
88 formation, and can live for at least 48 years. Such impressive longevity is not unusual for a high-
89 latitude species, as across the Bivalvia there is a tendency for lifespan to increase and growth rate
90 to decrease with higher latitude (Moss et al. 2016), though the pattern is often complex (Reed et
91 al. 2021). *Astarte borealis* is a common component of many Arctic and boreal seas so
92 understanding its life history strategy across its distribution will provide further understanding of
93 high-latitude ecosystems and perhaps identify areas where it can be used as a biomonitor (e.g.,
94 Boening 1999; Dunca et al. 2005; Gillikin et al. 2005; Black et al. 2017). Though *A. borealis*
95 from the White Sea experiences summer growth slow downs, it is not uncommon in bivalves and
96 some gastropods that the timing of annual increment formation varies with latitude within a
97 species (e.g., Jones et al. 1989; Quitmyer et al. 1997; Elliott et al. 2003, Surge et al. 2013); this
98 could also be confirmed in *A. borealis* by comparing oxygen isotope ratios in different
99 populations. One impediment to this end is that the size of *A. borealis* varies throughout its
100 distribution. For example, indviduals from the White Sea (max 35.5 mm length; Moss et al.
101 2018) are typically bigger than those from the Baltic Sea (max 28.7 mm length; Zettler 2002).
102 However, because Baltic Sea *A. borealis* are smaller than their northern counterparts, traditional
103 micromilling techniques cannot be used to identify the seasonal timing of annual growth

104 increments or evaluate whether the season of slowed growth is similar to *A. borealis* from the
105 White Sea or more typical of other bivalve and limpet species inhabiting cold-temperate to
106 boreal biogeographic zones. Here, we employ secondary ion mass spectromety (SIMS) to
107 overcome this issue. SIMS allows for a horizontal sampling resolution of 10 μm with a sampled
108 mass of approximately a nanogram, orders of magnitude smaller than traditional micromilling
109 and IRMS methods. SIMS has been applied to modern marine bivalves (e.g., Dunca et al., 2009;
110 Olson et al., 2012; Vihtakari et al., 2016), as well as to both modern and fossil marine organisms
111 that accrete carbonate hard parts (e.g., Kozdon et al., 2009; Matta et al. 2013; Helser et al.
112 2018a, 2018b; Linzmeier et al. 2018; Wycech et al., 2018). Using this technique, here we find
113 that annual growth slow downs, which result in the formation of dark growth increments as
114 viewed in cross section, can occur in fall, winter, or spring (like many other bivalves from cold-
115 temperate to boreal habitats but unlike *A. borealis* from the White Sea) and that individuals from
116 the Baltic Sea are quite long-lived (up to 43 years) and slow growing.
117
118 **Ecology**
119 The aragonite bivalve *A. borealis* has a circumpolar panarctic distribution. In the Atlantic
120 Ocean it has been reported from Newfoundland to Massachusetts Bay and Greenland to Iceland.
121 It is also found along the Pacific Coast of Alaska and British Columbia, as well as the Arctic
122 Seas around Russia and in the Baltic Sea from Germany to Poland (Zettler 2001). *Astarte*
123 *borealis* is an extremely shallow burrower and is an infaunal suspension feeder. It prefers
124 substrates of muddy-sand containing gravel (Saleuddin 1965) and is typically found between 0
125 and 300 m water depth (Zettler 2002). Due to low salinities and brackish waters in some areas of
126 the Baltic Sea (e.g. Bornholm Basin, eastern Gotland Basin), *A. borealis* lives in deeper regions

with higher salinity. The optimal salinity range lies between 14 and 30 practical salinity units (psu) (Oertzen, 1973). It can survive in salinities between 10 and 15 psu with its minimum tolerance at 6-8 psu. In the Baltic Sea densities of up to 1,000 individuals/m^2 and a wet weight up to 1.3 kg/m^2 (or 80 g/m^2 ash-free dry weight) were observed (unpublished data from the IOW Benthos Data Base, Leibniz Institute for Baltic Sea Research Warnemünde). Compared to other areas of origin, the spawning season of *A. borealis* in the Baltic Sea shows an extremely long period of mature eggs and sperm, with a maximum in winter and spring season (Oertzen 1972).

Materials and Methods

Study area

Samples used in our anlaysis were collected alive by one of the authors from 2001-2003 for use in previous studies to understand the benthic ecology and distribution of marine species in the Baltic Sea (Zettler 2002). We focused our efforts on two closely spaced localilties from different depths in the southwestern Baltic Sea (Fig. 1); RFP3S, depth = 20.9 m, salinity =16.7 psu, WA, depth = 31.3 m, salinity = 8.3 psu. Samples were collected with a van Veen grab. Biological tissue was preserved in the samples but was removed for sclerochronologic analyses. The samples were first fixed on board in formaldehyde (4%) and later stored in ethanol (70%). Shell height (anterior to poster) measurements were made using a digital caliper (to one significant digit) to compare sizes of individuals between the two populations examined here and also other studied populations.

Shell preparation and oxygen isotope analysis

149 Aragonite shells were cut along the maximum axis of growth to reveal growth increments
150 (Fig. 2). One specimen was selected from the RFP3S population for SIMS anlysis (specimen
151 number RFP3S-59) and cast in a 2.5 cm diameter and 4 mm thick round epoxy mount along with
152 multiple grains of the calcite standard UWC-3 ($\delta^{18}O$ = 12.49‰ Vienna Standard Mean Ocean
153 Water, VSMOW; Kozdon et al. 2009). The mount was sent to Wagner Petrographic for polishing
154 down to 0.05 μm grit using a diamond polishing compound after which it was sputter coated
155 with gold ~60 nm thick prior to SIMS analysis.
156 SIMS analysis was completed at the University of Wisconsin-Madison WiscSIMS lab on
157 a Cameca IMS 1280. Instrumental parameters followed Wycech et al. (2018). A 1.0 nA primary
158 beam of $^{133}Cs^{+}$ sputtered analysis pits ~10 μm in diameter and ~1 μm deep. Sputtered secondary
159 ions of $^{16}O^{-}$, $^{18}O^{-}$ and $^{16}OH^{-}$ were detected simultaneously on three Faraday detectors, with
160 secondary $^{16}O^{-}$ count rates of ~2.4 Gcps. Oxygen isotope ratios ($\delta^{18}O$) of the shell are reported in
161 permil units (‰) relative to the VPDB (Vienna Pee Dee Belemnite) standard. Precision was
162 calculated as the 2 s.d. of repeated groups of bracketing measurements on the calcite running
163 standard UWC-3, which averaged ±0.24‰ (2 s.d.) across the analysis session. For each group of
164 10-15 aragonite sample analyses, measured (raw) values of $\delta^{18}O$ were corrected to the VPDB
165 scale in three steps. First, the bracketing measurements of UWC-3 were used to calculate the
166 instrumental bias of calcite on VSMOW scale. Then, an adjustment for the small difference in
167 instrumental bias (0.88‰) between calcite and aragonite analysis was applied based on
168 calibration analyses of aragonite standard UWArg-7 ($\delta^{18}O$ = 19.73‰ VSMOW, Linzmeier et al,
169 2016 completed at the beginning of the analysis session. Last, conversion from the VSMOW to
170 the VPDB scale followed Coplen et al. (1993).

Sampling started within the middle microstructural layer ~8.5 mm from the umbo at approximately the 12th couplet of light and dark growth increments. The early portion of this shell was lost to taphonomic processes, which forced us to choose a location with more visible growth increments with adequate spacing. Sampling proceeded by manual site selection along growth direction. Adjustments in the location of sampling paths across growth increments were made to maintain perpendicular direction relative to growth lines (Fig. 3A). In addition, we analyzed a series of SIMS sample pits (n = 8) along a single growth line from the middle to outer microstructural layers representing coeval precipitation to evaluate lateral variability in oxygen isotope ratios (Fig. 3B). A total of 137 pits were generated representing ~4 mm of growth. See supplemental data archived in the Center for Open Source Science repository (https://osf.io/) for detailed reporting of all SIMS results.

After analysis, SIMS data were subjected to quality controls. First, analytical metrics of each sample measurement – including secondary ion yield, $^{16}OH^{-}/^{16}O^{-}$ ratio, and internal variability – were compared to the mean of the bracketing standards to confirm their quality. Scanning electron microscopy (SEM) of SIMS analysis pits were made to screen for irregular pit shapes that may bias the $\delta^{18}O$ data. The epoxy sample discs were mounted onto aluminum mounts with double-sided copper tape. Images were taken using a Zeiss Supra 25 FESEM operating at 5.5kV, using the SE2 detector, 30µm aperture, and working distances of 12 to 15 mm (Carl Zeiss Microscopy, LLC, Peabody, MA). SEM images of SIMS analysis pits revealed no irregularities of either pit morphology or aragonite substrate (Fig. 3C). In total, five SIMS spots were eliminated as outliers, and the remaining 132 are hereafter included in figures and discussion.

193 Next, we prepared the surface of specimen number RFP3S-59 for micromilling and
194 traditional IRMS analysis as a coarse comparison to the ultra-high-resolution SIMS data. The
195 specimen was repolished on a Buehler MetaServ 2000 variable speed grinder-polisher using
196 diamond suspension solutions of 6 and 1 µm to remove the gold coating. Micromilling was
197 perfomed on a Merchantek micromilling system fitted with a Brasseler tungsten carbide dental
198 scriber point (part number H1621.11.008) and digitized paths followed 8 dark increments that
199 overlapped the SIMS sampling path. Six of these samples yielded sufficient amounts of
200 carbonate powder for analysis at the Environmental Isotope Laboratory, University of Arizona.
201 Samples were reacted with dehydrated phosphoric acid under vacuum at 70 ºC for 1 hour and
202 exolved CO_2 gas was analyzed with an auto carbonate reaction system (Kiel-III Devise) coupled
203 to a Finnigan MAT 252 IRMS. Isotope ratios were calibrated based on repeated measurements of
204 NBS-18 (National Bureau of Standards) and NBS-19 and no differential acid fractionation factor
205 was applied to account for aragonite samples versus calcite standards. Precision is ±0.1‰ (1σ)
206 for $\delta^{18}O$ values based on repeated measurement of internal carbonate standards. IRMS $\delta^{18}O$
207 values are also reported relative to the VPDB carbonate standard.
208
209 *Visualization of growth increments*
210 Thick sections of shells (approximatley 1-2 cm) for all individuals from each population
211 (RFP3S, n= 67; WA, n=40) were made to visualize growth increments (Fig. 2). The shells of *A.*
212 *borealis* are thin and delicate so to prevent cracking during cutting, shells were first embedded
213 with an epoxy. We experimented with two different epoxy materials. The first was Castolite AC
214 from EagerPolymers (www.eagerpolymers.com). In this method, shells were placed in silicone
215 muffin baking trays and covered in resin. The resin did not stick to the silicone surface, so

embedded shells would come out easily. This approach proved successful in protecitng the shells, but much resin was wasted as the muffin trays were larger than the shells themselves. To remedy this situation, we used a simple two-part syringe Gorilla Glue® clear epoxy and coated the shells in a single layer and then allowed them to cure on wax paper for twenty-four hours in a fume hood. After epoxy, shells were cut with Buehler Isomet low-speed saw along the axis of maximum growth to reveal internal increments. Thick sections of the shell were then glued onto a glass slide and polished on a Buehler MetaServ 2000 variable speed grinder-polisher by first using a 600 grit silicon carbide disc and finishing with diamond suspension solutions of 6 and 1 µm. Polished thick sections were imaged with an Olympus SZX7 steromicroscope system coupled with an Olympus DP71 12.5 megapixel digital camera. A series of images were taken from umbo to commissure of each thick section and stitched together using Olympus Stream Essentials Software version 2.2. We then measured the cumulative widths of growth increments along the outer shell layer from umbo to commissure using Olympus Software. These widths were then transformed to a straight line distance by dividing each value by the total cumulative width and multiplying that by the overall shell height as measured using a digital caliper. This approach allows growth curves to be invesitaged in the context of shell heights measured for an entire popluation.

After all growth increments were measured for each population, we fit the von Bertalanffy growth equation (von Bertalanffy 1938, VBG) to the pooled size-at-age data using the non-linear least squares (nls) procedure in the open source R language (cran.r-project.org). VBG describes the size of an individual at an give time (H_t):

$$H_t = H_\infty (1 - e^{-k(t-t_0)})$$

where H_∞ = the asymptotic size, t_o = the time at which H_t=0, and k = the rate at which H_∞ is approached. The factor, k, is an important, but often misconstrued parameter of the VBG. In practice, a k value for any species of bivalve cannot be used to determine an exact amount of shell material accreted in a given year because k is in units of year^{-1}. In addition, k is in part dependent on H_∞ so individuals with identical k values, but different H_∞ values would acrete different amounts of shell in a given year. Additionally, inverse plots of age versus cumulative size reveal that increments added throughout ontogeny decrease in their width at an exponential rate. Thus, higher k values represent a faster approach to smaller growth increments.

Results

Oxygen Isotope Analyses

The SIMS $\delta^{18}O$ time series of specimen RFP3S-59 exhibits a quasi-sinusoidal trend with relatively sharp peaks (high values) and valleys (low values) over nine clear cycles (Fig. 4). Values range from −5.9 to −3.3‰ and the average and 1 s.d. of the amplitude of the nine $\delta^{18}O$ cycles is 2.1±0.3‰. The six IRMS $\delta^{18}O$ values that were sampled at a much coarser scale and centered on dark increments had notably higher $\delta^{18}O$ values ranging from −2.59 to −2.12‰, with average and 1 s.d. of −2.4±0.2‰.

The lowest $\delta^{18}O$ values are consistently associated with light increments in the time series measured by SIMS; however, the location of dark increments relative to the SIMS $\delta^{18}O$ time series is more complicated (Figs. 3B and 4). Many of the dark increments coincide with higher $\delta^{18}O$ values, whereas some occur where values are increasing and others where values are

decreasing. To test lateral variability, $\delta^{18}O$ values were measured in eight spots along a single growth increment from the middle to outer microstructural layer (Fig. 3B). Within the middle microstructural layer, $\delta^{18}O$ values ranged from –3.7 to –3.3‰ with an average of –3.4‰ (n = 6) and spot-to-spot reproducibility (±0.3‰ 2 s.d.) comparable to the running standard. The two $\delta^{18}O$ measurements in the outer microstructural layer were slightly more negative, each measuring –4.0‰.

Size, lifespan and growth

Measurements of shell height (Fig. 5A and 5B) showed no apparent differences in sizes between the RFP3S and WA populations. Our shell measurements compare well to those of previous studies in the Baltic Sea (Zettler 2002), though the smallest size fraction of our sample proved too difficult to work with for sclerochronologic studies so they were not included.

Thin, dark, annual growth increments identified by their consistent occurrence at or near peak $\delta^{18}O$ values using SIMS allowed for the determination of lifespan and growth of each population. Because the two populations have similar size distributions, it was no surprise that their age distributions were similar as well (Fig. 5C and 5D). In both populations, most individuals fall between 10 and 40 years in age at the time of collection, with peak abundances between 20-30 years.. The maximum ages of each population are similar at 43 (RFP3S) and 41 (WA). In addition to similar age distributions, the VBG growth equations do not vary significantly either. Both populations have low k (0.08 RFP3S, and 0.06 WA) and H_∞ values (16.12 mm RFP3S, 19.81 mm WA) and thus exhibit relatively slow growth to a small size (Fig. 7).

Discussion

Annual Growth Checks

Isotope sclerochronology using IRMS analysis of $\delta^{18}O$ values has long been established as a reliable method for determining seasonal variation in growth rates of bivalve shells (e.g., Jones and Quitmyer 1996; references in Schöne and Surge, 2012). Our findings show that for bivalve shells that are small, slow growing, and long-lived and have extremely narrowly spaced growth increments, SIMS $\delta^{18}O$ analysis provides a reliable method for establishing seasonal growth checks and ontogenetic age that is otherwise unattainable. Oxygen isotope ratios sampled from the middle microstructural layer along a coeval growth line are statistically similar with a 2 s.d. comparable to the UWC-3 running standard. In comparison, the two samples taken from the outer microstructural layer were slightly more negative. Therefore, best SIMS practice is to test the variability along a coeval growth line, similar to a Hendy (1971) test in speleothems, and use that assessment to guide the time-series sampling in the direction of growth.

Our relatively small number of coarsely micromilled IRMS samples showed higher average $\delta^{18}O$ values compared to the SIMS $\delta^{18}O$ data. Although characterizing the cause of the offset between SIMS and IRMS $\delta^{18}O$ results is beyond the scope of this study, earlier studies have also documented offsets (also with SIMS $\delta^{18}O$ lower than IRMS $\delta^{18}O$) in low-temperature carbonates (Orland et al., 2015; Helser et al., 2018b; Wycech et al., 2018). Helser et al. (2018b) measured a ~0.5‰ offset in aragonitic fish otoliths, but found that SIMS more clearly captured seasonal $\delta^{18}O$ variation than micromilling/IRMS. Helser et al. (2018b) also note a negative correlation of $^{16}OH^-/^{16}O^-$ and $\delta^{18}O$ values in SIMS measurements of their otolith and build on prior work (Orland et al., 2015; Wycech et al., 2018) in suggesting that a possible cause of this correlation is the inclusion of water and/or organic matter in the sample; by this hypothesis,

increased water and/or organic content would cause SIMS analyses to have lower $\delta^{18}O$ values. By nature of the analytical techniques, these components could be included in SIMS $\delta^{18}O$ measurements but are excluded from IRMS. Interestingly, in this study there is a weak positive correlation ($r^2 = 0.21$) of $^{16}OH^-/^{16}O^-$ and $\delta^{18}O$ values across all sample analyses. A notable exception to this trend is a strong negative correlation ($r^2 = 0.91$) of $^{16}OH^-/^{16}O^-$ and $\delta^{18}O$ values for the eight analyses along a single growth increment. No data exist, however, that quantitatively characterize the correlation of $\delta^{18}O$ and $^{16}OH^-/^{16}O^-$or the $\delta^{18}O$ offset to water and/or organic inclusions, and establishing causation of these observations in SIMS analysis of biocarbonates is an ongoing challenge. Thus, the interpretations discussed below rely solely on the relative values and variability of SIMS $\delta^{18}O$ analyses and not the absolute $\delta^{18}O$ values. The quasi-sinusoidal trend in the SIMS $\delta^{18}O$ time series likely reflects seasonal variation and demarcates annual changes in shell growth patterns representing 9 years of growth. Although difficult to quantify without detailed water temperature and $\delta^{18}O_{water}$ values during the growth period, we hypothesize that the seasonal signal likely reflects seasonal temperature change with lower $\delta^{18}O$ corresponding to summer growth. This will be the subject of a forthcoming paper. Several biological processes and environmental conditions have been reported to influence seasonal variation in shell growth, including reproduction/spawning, food supply, and minimum/maximum temperature thresholds lowering metabolic rates (e.g., Jones et al. 1983; Jones and Quitmyer, 1996; Lutz and Rhoads 1980; Richardson 2001; Sato, 1995; Schöne et al. 2005b). Shifts in the seasonal timing of slowed growth along a latitudinal gradient have been documented in many bivalve and limpet groups. Individuals collected along the eastern seaboard of the United States from Florida to New York (Jones et al. 1989; Quitmyer et al. 1997; Elliott et al. 2003) and along the western North Atlantic from northern Spain to Norway (Surge et al.

2013) form dark annual increments/growth checks during summer and those from mid to high latitudes form dark annual increments/growth checks during winter. The authors propose that temperature thresholds are the most likely explanation for the latitudal shift in the timing of slowed growth. In a meta-analysis of bivalve growth seasonality, Killam and Clapham (2018) found that winter growth slow downs are common in polar bivalves, whereas summer slow downs are typical of mid-latitude species. This latitudinal pattern can be more complicated, however. Henry and Cerrato (2007) observed changes in the timing of dark increment formation in the northern hard clam, *Mercenaria mercenaria*, from Narragansett Bay, Rhode Island, USA, over a period of more than two decades. Earlier harvested individuals formed the expected dark increment in winter but the timing switched to a more complicated pattern with multiple dark increments in a single year. They hypothesized a human-induced change in environmental conditions within the watershed may be responsible for the more complicated growth pattern in *M. mercenaria* shells through time. The extremely long-lived ocean quahog, *Arctica islandica*, from the cold waters of the North Atlantic is known to form annual growth checks about one month after the maximum water temperature, but the time of formation depends on whether the individual lives above or below the thermocline (Schöne 2013). The timing of annual growth checks in this species can also be influenced by food availability, which becomes limited between fall and spring (Ballesta-Artero et al., 2017).

Moss et al. (2018) used isotope sclerochronology to decipher annual growth patterns in *A. borealis* from a population in the White Sea, Russia. There, clear couplets of light/dark increments were hypothesized to form annually and large enough to analyze using traditional micromilling/IRMS techniques. Despite the high latitude, dark increments did not form in winter as expected and instead formed during summer. Using circumstantial evidence, Moss et al.

354 (2018) reasoned that the most likely explanation for this unexpected pattern may correspond to
355 the late summer spawning period in the White Sea. The specimen analyzed in our study from the
356 Baltic Sea shows a more complicated pattern. Dark increments occur during cold or cool months
357 (higher $\delta^{18}O$) and can begin formation during fall (cycles 1-4), winter (cycles 5 and 8), or spring
358 (6, 7, and 9) (Fig. 4). Summers (lower $\delta^{18}O$) are consistently associated with relatively wider,
359 lighter colored growth increments that suggest faster growth, although light increments are also
360 observed to commence in cooler months (cycles 1-4) and last into winter (cycles 5-9). Thus,
361 temperature stress could explain the growth slow down in *A. borealis* from the Baltic Sea like it
362 does in many bivalve species at high latitudes (Killam and Clapham 2018) but it likely is not the
363 sole factor driving seasonal changes in growth rate. Spawning events can also result in annual
364 increment formation, and *A. borealis* have been found with mature eggs and sperm in both
365 winter and spring in the Batlic (Oertzen, 1972), so that cannot be ruled out as a possibility. In
366 addition, the individual sampled here appears to show a trend of seasonal slow downs shifting
367 from fall to spring months later in ontogeny (Figures 3, 4). Given the complicated timing of
368 annual increments, we suggest that oxygen isotope data be collected from additional specimens
369 to test these hypotheses.
370
371 *Life history*
372 Modern bivalves generally show an increase in lifespan and a decrease in von Bertalanffy
373 k with latitude (Moss et al. 2016), a pattern that holds across Bivalvia and within groups.
374 Patterns within *A. borealis* appear to be more complex. Though this may be because methods for
375 determining lifespans of *A. borealis* throughout its range are almost as varied as the reported
376 lifespans themselves. At its northernmost limits, traditional isotope sclerochronology has shown

A. borealis to be be exceptionally long-lived, reaching 150 years in Greenland (Torres et al. 2011) and 48 years in the White Sea (Moss et al. 2018). Our results of over 40 years in the Baltic Sea are not unexpected. To our knowledge, lifespans of *A. borealis* from the Baltic Sea have only been reported from Gusev and Rudinskaya (2014) at "greater than 10 years." However, their study was not guided by isotope sclerochronology and their methods for determining annual growth increments are unclear. Elsewhere, several other studies have shown much shorter maximum lifespans (8-10 years) from the Sea of Okhotsk and the Eastern Siberian Sea (Gagayev 1989; Selin 2007, 2010). These studies though used ridges on the external shell surface instead of internal growth increments. External shell ridges are often problematic in determining lifespans of bivalves as they can be the result of disturbance events like storms, rather than from periodic events (Krantz et al. 1984).

Our results emphasize the need for using isotope sclerochronology to undertsand the true lifespan range of *A. borealis* throughout its distribution. While traditional methods are often not possible on small, slow growing, and long-lived species, we demonstrate that SIMS provides a reliable method to determine the periodicity of growth increment formation. Furthermore, our data suggest that *A. borealis* could potentially act as not only a biomonitor, but also a climate recorder using both live and dead collected samples (Boening 1999; Szefer 2002) as the species has a long history in the Baltic Sea. The Baltic Sea has a long and complex anthropogenic pollution history and several short- and long-lived bivalves have contributed to understanding these patterns (Szefer and Szefer 1990; Rainbow et al. 2004; Liehr et al. 2005; Protasowicki et al. 2008; Hendozko et al. 2010; Schöne et al. 2021). Finally, while life history information is available for a signifiant number of species, data currently appear to be skewed to larger, more

commerically important groups. Oxygen isotope data determined using SIMS provides a mechanism to resolve this gap and to better understand benthic marine communities.

Compliance with Ethical Standards

Acknowledgments

We thank Garrett Braniecki for drafting the map figure. Comments from two anonymous reviewers improved the manuscript. Funding for this study was provided by the US National Science Foundation (NSF) to Surge (grant #EAR-1656974). The WiscSIMS Laboratory is supported by the US NSF (grant # EAR-1355590 and EAR-1658823).

References

Ballesta-Artero I, Witbaard R, Carroll ML, van der Meer J (2017) Environmental factors regulating gaping activity of the bivalve *Arctica islandica* in Northern Norway. Marine Biology 164: 116. doi: 10.1007/s00227-017-3144-7

Barker RM (1964) Microtextural variation in pelecypod shells. Malacologia 2:69–86.

Black HD, Andrus CFT, Lambert WJ, Rick TC, Gillikin DP (2017) $\delta^{15}N$ values in *Crassostrea virginica* shells provides early direct evidence for nitrogen loading to Chesapeake Bay. Sci Rep 7:3–10. doi: 10.1038/srep44241

Boening DW (1999) An evaluation of bivalves as biomonitors of heavy metals pollution in marine waters. Environ Monit Assess 55:459–470.

Clark GR (1974) Growth lines in invertebrate skeletons. Annu Rev Earth Planet Sci 2:77–99. doi: 10.1146/annurev.ea.02.050174.000453

Coplen TB, Kendall C, and Hopple J (1983) Comparison of stable isotope reference samples. Nature 302: 236-238.

Dunca E, Schöne BR, Mutvei H (2005) Freshwater bivalves tell of past climates: But how clearly do shells from polluted rivers speak? Palaeogeogr Palaeoclimatol Palaeoecol 228:43–57. doi: 10.1016/j.palaeo.2005.03.050

Dunca E, Mutvei H, Göransson P, Morth CM, Schone BR, Whitehouse MJ, Elfman M, Baden SP. (2009) Using ocean quahog (*Arctica islandica*) shells to reconstruct palaeoenvironment in Öresund, Kattegat and Skagerrak, Sweden. Int J Earth Sci (Geol Rundsch) 98:3-17

Elliot M, deMenocal PB, Linsley BK, Howe SS (2003) Environmental controls on the stable isotopic composition of *Mercenaria mercenaria*: potential application to paleoenvironmental studies. Geochemistry Geophysics Geosystems 4: 1-16. doi:

446 10.1029/2002GC000425
447 Gagayev S (1989) Growth and production of mass ppecies of bivalves in Chaun Bay (East
448 Siberian Sea). Oceanology 29:504–507.
449 Gillikin DP, Dehairs F, Baeyens W, Navez J, Lorrain A, André L (2005) Inter- and intra-annual
450 variations of Pb/Ca ratios in clam shells (*Mercenaria mercenaria*): A record of
451 anthropogenic lead pollution? Mar Pollut Bull 50:1530–1540. doi:
452 10.1016/j.marpolbul.2005.06.020
453 Goodwin DH, Flessa KW, Schöne BR, Dettman DL, Schöne BR (2001) Cross-calibration of
454 daily growth increments, stable isotope variation, and temperature in the Gulf of California
455 bivalve mollusk *Chione cortezi*: Implications for paleoenvironmental analysis. Palaios
456 16:387–398. doi: 10.1669/0883-1351(2001)016
457 Gusev AA, Rudinskaya LV (2014) Shell form, growth, and production of Astarte borealis
458 (Schumacher, 1817) (Astartidae, Bivalvia) in the southeastern Baltic Sea. Oceanology
459 54:458–464. doi: 10.1134/S0001437014040043
460 Helser T, Kastelle C, Crowell A, Ushikubo T, Orland IJ, Kozdon R, Valley JW (2018a) A 200-
461 year archaeozoological record of Pacific cod (*Gadus macrocephalus*) life history as
462 revealed through ion microprobe oxygen isotope ratios in otoliths. J Archaeol Sci Reports
463 21:1236–1246. doi: 10.1016/j.jasrep.2017.06.037
464 Helser TE, Kastelle CR, McKay JL, Orland IJ, Kozond R, Valley JW (2018b) Evaluation of
465 micromilling/conventional isotope ratio mass spectrometry and secondary ion mass
466 spectrometry of δ18O values in fish otoliths for sclerochronology. Rapid Commun Mass
467 Spectrom 32:1781–1790. doi: 10.1002/rcm.8231
468 Hendozko E, Szefer P, Warzocha J (2010) Ecotoxicology and Environmental Safety Heavy

metals in *Macoma balthica* and extractable metals in sediments from the southern Baltic Sea. Ecotoxicol Environ Saf 73:152–163. doi: 10.1016/j.ecoenv.2009.09.006

Hendy CH (1971) The isotopic geochemistry of speleothems — I. The calculation of the effects of different modes of formation on the isotopic composition of speleothems and their applicability as paleoclimate indicators. Geochim. Cosmochim. Acta 35: 801–824.

Henry KM, Cerrato RM (2007) The annual macroscopic growth pattern of the northern quahog [=hard clam, *Mercenaria mercenaria* (L.)], in Narragansett Bay, Rhode Island. J. Shellfish Res. 26: 985-993. doi 10.2983/0730-8000(2007)26[985:tamgpo]2.0.co;2

Jones DS, Quitmyer IR (1996) Marking time with bivalve shells: oxygen isotopes and season of annual increment formation. Palaios 11:340. doi: 10.2307/3515244

Jones DS, Williams DF, Arthur MA (1983) Growth history and ecology of the Atlantic Surf Clam, *Spisula solidissima* (Dillwyn), as revealed by stable isotopes and annual shell increments. J Exp Mar Biol Ecol 73:225–242. doi: 10.1016/0022-0981(83)90049-7

Jones DS, Arthur MA, Allard DJ (1989) Sclerochronological records of temperature and growth from shells of *Mercenaria mercenaria* from Narragansett Bay, Rhode Island. Mar. Biol 102: 225-234 doi: 10.1007/BF00428284

Killam, DE, Clapham ME. (2018) Identifying the ticks of bivalve shell clocks: seasonal growth in relation to temperature and food supply. *Palaios*, 33, 228-236. doi:10.2110/palo.2017.072

Kozdon R, Ushikubo T, Kita, NT, Spicuzza MJ, & Valley, JW (2009) Intratest oxygen isotope variability in the planktonic foraminifer *N. pachyderma*: Real vs. apparent vital effects by ion microprobe. Chem. Geol, 258(3–4), 327–337.

Krantz DE, Jones DS, Williams DF (1984) Growth rates of the sea scallop, *Placopecten*

492 *magellanicus*, determined from the $^{18}O/^{16}O$ record in shell calcite. Biol Bull 167:186–199.
493 Liehr G, Zettler ML, Leipe T, Witt G (2005) The ocean quahog *Arctica islandica* L. - A
494 bioindicator for contaminated sediments. Mar Biol 147:671–679.
495 Linzmeier BJ, Kozdon R, Peters SE, Valley JW (2016) Oxygen isotope variability within
496 *Nautilus* shell growth bands. PLoS ONE 11(4): e0153890.
497 doi:10.1371/journal.pone.0153890
498 Linzmeier ABJ, Landman NH, Peters SE, Kozdon R, Kitajima K (2018) Ion microprobe –
499 measured stable isotope evidence for ammonite habitat and life mode during early
500 ontogeny. Paleobiology 44:684–708. doi: 10.1017/pab.2018.21
501 Lutz, RA, and Rhoads, DC (1980) Growth patterns within the molluscan shell. In Rhoads DC
502 and Lutz, RA (eds) Skeletal growth of aquatic organisms. Plenum Press, New York, pp.
503 203-254.
504 Matta ME, Orland IJ, Ushikubo T, Helser TE, Black BA, Valley JW (2013) Otolith oxygen
505 isotopes measured by high-precision secondary ion mass spectrometry reflect life history of
506 a yellow fin sole (*Limanda aspera*). Rapid Commun Mass Spectrom 27:691–699. doi:
507 10.1002/rcm.6502
508 Moss DK, Ivany LC, Judd EJ, Cummings PW, Bearden CE, Kim WJ, Artruc EG, Driscoll JR
509 (2016) Lifespan, growth rate, and body size across latitude in marine bivalvia, with
510 implications for Phanerozoic evolution. Proc R Soc B Biol Sci. 283. doi:
511 10.1098/rspb.2016.1364
512 Moss DK, Surge D, Khaitov V (2018) Lifespan and growth of *Astarte borealis* (Bivalvia) from
513 Kandalaksha Gulf, White Sea, Russia. Polar Biol 41:1359–1369. doi: 10.1007/s00300-018-
514 2290-9

515 Oertzen J-A von (1972) Cycles and rates of reproduction of six Baltic Sea bivalves of different
516 zoogeographical origin. Mar Biol 14:143–149.
517 Oertzen J-A von (1973) Abiotic potency and physiological resistance of shallow and deep water
518 bivalves. Oikos Suppl 15:261–266.
519 Olson IC, Kozdon R, Valley JW and Gilbert PUPA (2012) Mollusk shell nacre ultrastructure
520 correlates with environmental temperature and pressure. J.Am. Chem. Soc. 134, 7351-7358.
521 Orland IJ, Kozdon R, Linzmeier B, et al. Enhancing the accuracy of carbonate δ18O and δ13C
522 measurements by SIMS. American Geophysical Union, Fall Meeting, December 18, 2015.
523 Presentation PP52B-03. https://agu.confex.com/agu/fm15/meetingapp.cgi/Paper/67486
524 (accessed April 12, 2021)
525 Pannella G (1976) Tidal growth patterns in recent and fossil mollusc bivalve shells. Sci. Nat.
526 Heidelberg 63:539–543.
527 Pannella G, MacClintock C (1968) Biological and environmental rhythms reflected in molluscan
528 shell growth. Paleontol Soc Mem 2:64–80.
529 Protasowicki M, Dural M, Jaremek J (2008) Trace metals in the shells of blue mussels (*Mytilus*
530 *edulis*) from the Poland coast of Baltic sea. Environ Monit Assess 141:329–337. doi:
531 10.1007/s10661-007-9899-4
532 Quitmyer IR, Jones DS, Arnold WS (1997) The sclerochronology of hard clams, *Mercenaria*
533 spp., from the South-Eastern U.S.A.: A method of elucidating the zooarchaeological records
534 of seasonal resource procurement and seasonality in prehistoric shell middens. J Archaeol
535 Sci 24:825–840. doi: 10.1006/jasc.1996.0163
536 Rainbow PS, Fialkowski W, Sokolowski A, Smith BD, Wolowicz M (2004) Geographical and
537 seasonal variation of trace metal bioavailabilities in the Gulf of Gdansk , Baltic Sea using

538 mussels (*Mytilus trossulus*) and barnacles (*Balanus improvisus*) as biomonitors. Mar Biol
539 144:271–286. doi: 10.1007/s00227-003-1197-2
540 Reed, AJ, Godbold, JA, Grange, LJ, and Solan, M 2021 Growth of marine ectotherms is
541 regionally constrained and asymmetric with latitude. Global Ecol Biogeogr 1-12. doi:
542 10.1111/geb.13245
543 Richardson, CA (2001) Molluscs as archives of environmental change. Oceanogr. Mar. Bio.
544 39:103–164.
545 Saleuddin ASM (1965) The mode of life and functional anatomy of *Astarte* spp.
546 (eulamellibranchia). J Molluscan Stud 36:229–257. doi:
547 10.1093/oxfordjournals.mollus.a064952
548 Sato, S (1995) Spawning periodicity and shell microgrowth patterns of the venerid bivalve
549 *Phacosoma japonicum* (Reeve, 1850). The Veliger 38:61–72
550 Schöne BR, Surge D (2012) Chapter 14. Bivalve sclerochronology and geochemistry. In: Seldon
551 P, Hardesty J, Carter JG, coordinator (eds) Part N, Bivalvia, Revised, Volume 1 Treatise
552 Online 46:1-24. University of Kansas, Paleontological Institute, Lawrence, Kansas.
553 Schöne BR (2013) *Arctica islandica* (Bivalvia): A unique paleoenvironmental archive of the
554 northern North Atlantic Ocean. Glob Planet Change 111:199–225. doi:
555 10.1016/j.gloplacha.2013.09.013
556 Schöne, B.R., Fiebig, J., Pfeiffer, M., Gleß, R., Hickson, J., Johnson, A.L.A., Dreyer, W.,
557 Oschmann, W. (2005a) Climate records from a bivalved Methuselah (*Arctica islandica*,
558 Mollusca; Iceland). Palaeogeogr Palaeoclimatol Palaeoecol 228:130-148. doi:
559 10.1016/j.palaeo.2005.03.049
560 Schöne BR, Houk SD, Freyre Castro AD, Fiebig J, Oschmann W, Kröncke I, Dreyer W. and

561 Gosselck F (2005b) Daily growth rates in shells of *Arctica islandica*: assessing sub-seasonal
562 environmental controls on a long-lived bivalve mollusk. Palaios 20:78–92
563 Schöne BR, Huang X, Zettler ML.; Zhao L, Mertz R, Jochum KP, Walliser EO (2021) Mn/Ca in
564 shells of *Arctica islandica* (Baltic Sea) – A potential proxy for ocean hypoxia? Est Coast
565 Shelf Sci 251:107257.
566 Schumacher, CF (1817) Essai d'un nouveau systeme des habitations des Vers testaces.
567 Copenhagen, 287 pp.
568 Selin NI (2007) Shell form, growth and life span of *Astarte arctica* and *A. borealis* (Mollusca:
569 Bivalvia) from the subtidal zone of northeastern Sakhalin. Russ J Mar Biol 33:232–237.
570 doi: 10.1134/S1063074007040050
571 Selin NI (2010) The growth and life span of bivalve mollusks at the northeastern coast of
572 Sakhalin Island. Russ J Mar Biol 36:258–269. doi: 10.1134/S1063074010040048
573 Surge D, Walker KJ (2006) Geochemical variation in microstructural shell layers of the southern
574 quahog (Mercenaria campechiensis): implications for reconstructing seasonality.
575 Palaeogeogr Palaeoclimatol Palaeoecol 237:182–190. doi: 10.1016/j.palaeo.2005.11.016
576 Surge D, Kelly G, Arnold WS, Geiger SP, Gowert AE (2007) Isotope sclerochronology of
577 *Mercenaria mercenaria, M. campechiensis* , and their natural hybrid form: Does genotype
578 matter? Palaios 23:559–565. doi: 10.2110/palo.2007.p07-056r
579 Surge D, Wang T, Gutiérrez-Zugasti I, Kelley PH (2013) Isotope sclerochronology and season of
580 annual growth line formation in limpet shells (*Patella vulgata*) from warm- and cold-
581 temperate zones in the eastern North Atlantic. Palaios 28: 386-393. doi:
582 10.2110/palo.2012.p12-038r
583 Szefer P (2002) Metal pollutants and radionuclides in the Baltic Sea - an overview. Oceanologia

584 44:129-178.
585 Szefer P, Szefer K (1990) Metals in molluscs and associated bottom sediments of the southern
586 Baltic. Helgol. Meeresunters 44:411–424.
587 Torres ME, Zima D, Falkner KK, Macdonald RW, O'Brien M, Schöne BR, Siferd T (2011)
588 Hydrographic changes in nares strait (Canadian Arctic Archipelago) in recent decades based
589 on $\delta^{18}O$ profiles of bivalve shells. Arctic 64:45–58. doi: 10.1016/j.jmb.2005.01.031
590 Vihtakari, M., Renaud, P. E., Clarke, L. J., Whitehouse, M. J., Hop, H., Carroll, M. L., &
591 Ambrose Jr, W. G. (2016). Decoding the oxygen isotope signal for seasonal growth patterns
592 in Arctic bivalves. Palaeogeogr Palaeoclimatol Palaeoecol 446:263-283.
593 von Bertalanffy L (1938) A quantitative theory of organic growth (Inquires on growth laws. II).
594 Hum Biol 10:181–213.
595 Weidman CR, Jones GA, Kyger (1994) The long-lived mollusc *Arctica islandica:* A new
596 paleoceanographic tool for the reconstruction of bottom temperatures for the continental
597 shelves of the northern North Atlantic Ocean. J Geophys Res 99:18305. doi:
598 10.1029/94JC01882
599 Wycech JB, Kelly DC, Kozdon R, Orland IJ, Spero HJ, Valley JW (2018) Comparison of δ18O
600 analyses on individual planktic foraminifer (*Orbulina universa*) shells by SIMS and gas-
601 source mass spectrometry. Chem. Geol. 483:119-130. doi 10.1016/j.chemgeo.2018.02.028
602 Zettler M (2001) Recent geographical distribution of the *Astarte borealis* species complex, its
603 nomenclature and bibliography (Bivalvia: Astartidae). Schr. Malakozool. 18:1–14.
604 Zettler ML (2002) Ecological and morphological features of the bivalve *Astarte borealis*
605 (Scumacher, 1817) in the Baltic Sea near its geographical range. J Shellfish Res 21:33–40.
606

607 **Figures and Tables**

608

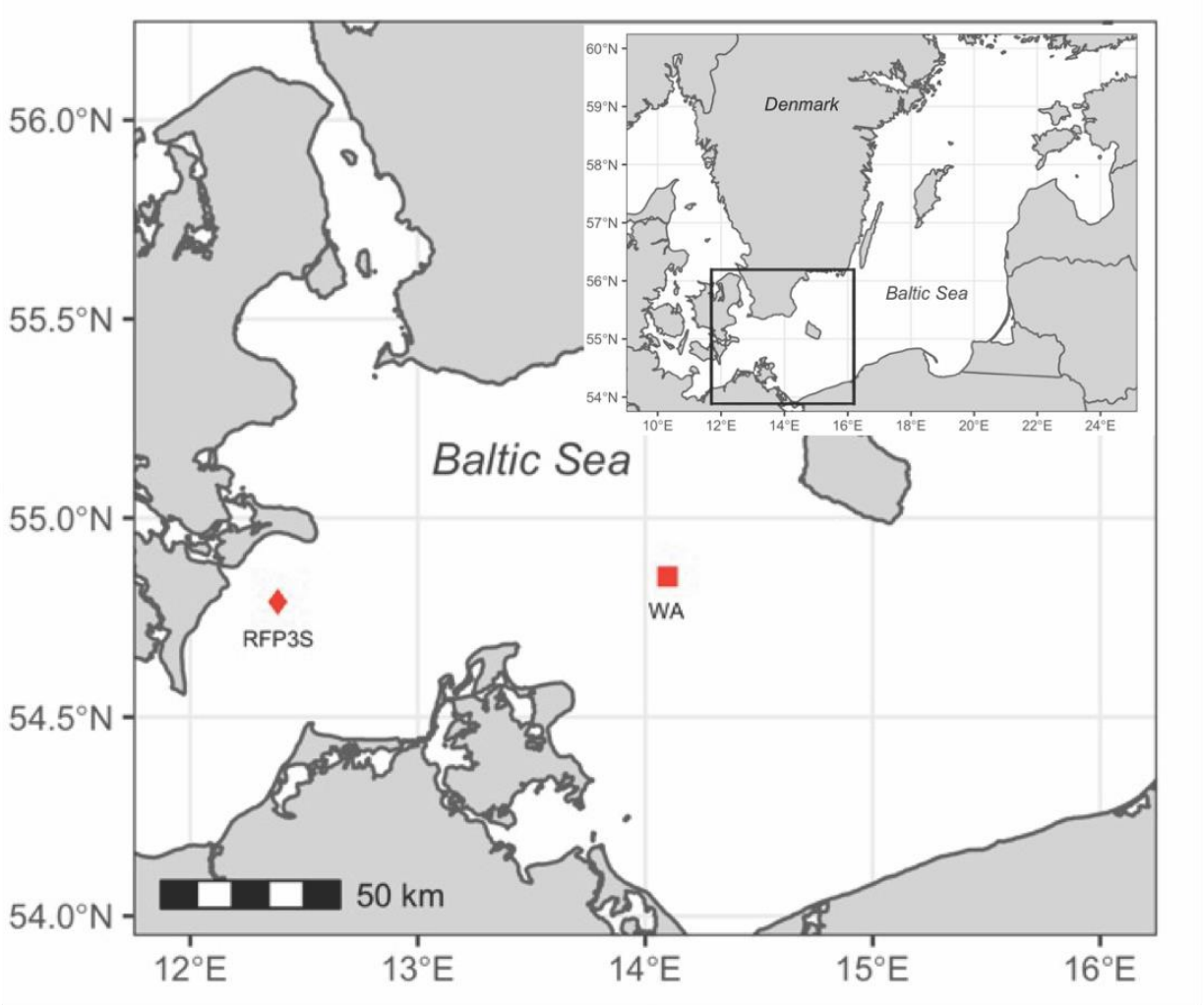

609

610 Figure 1. Location of the study sites in southeastern Baltic Sea region. RFP3S = 54.7967°N,

611 12.38787°E; WA = 54.86775°N, 14.09832°E. Shells were collected as part of a previous study

612 (Zettler 2002).

613

614

615

616

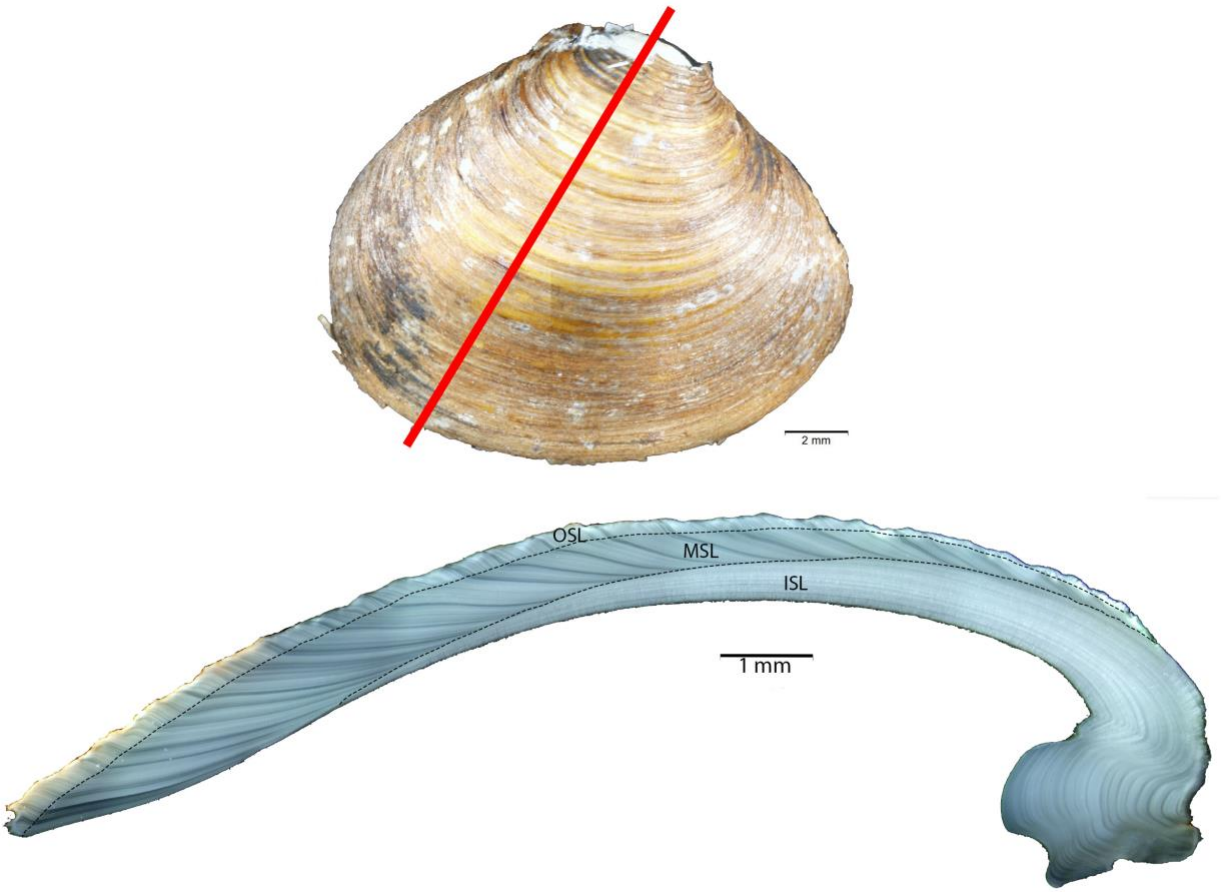

617

618 Figure 2. Upper image shows axis of maximum growth in RFP3S-47. Lower image is polished

619 cross section stitched together using Olympus software. Direction of growth is from right to left

620 in lower image. OSL= outer shell layer; MSL= middle shell layer; ISL= inner shell layer.

621

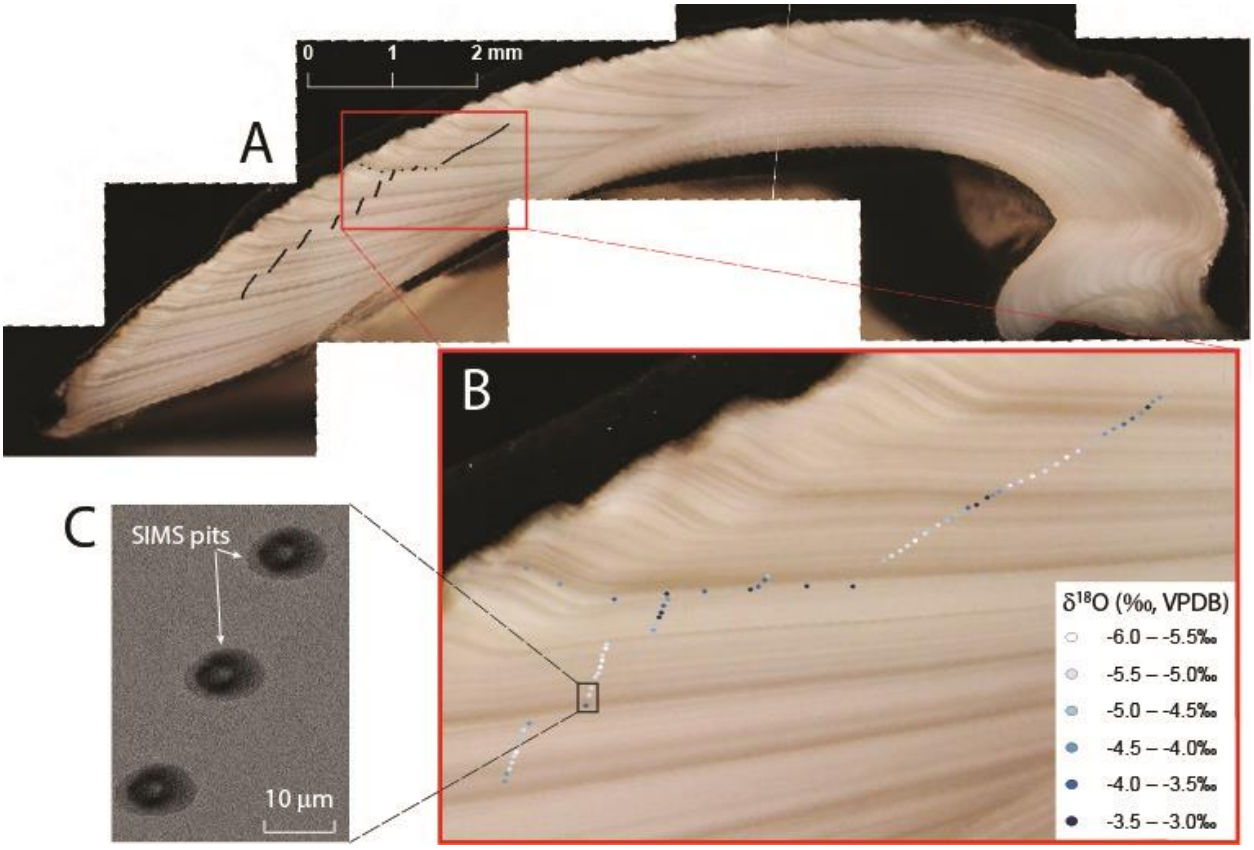

Figure 3. Photomicrograph and SEM images showing SIMS pits along sampling paths and associated $\delta^{18}O$ values. (A) Cross-section shell image show light and dark growth increments under reflected light. Black SIMS pits are enlarged from actual size to make them more visible. Growth direction is from right to left. Scale bar = 2 mm. (B) Enlarged image delineated by the red box on the shell cross-section showing color-coded ranges of SIMS $\delta^{18}O$ values in 0.5‰ intervals. The darker the blue, the higher the $\delta^{18}O$ values. (C) SEM images of SIMS sampling pits at high resolution (5.5k magnification) showing examples of no irregularities. Scale bar = 10 µm.

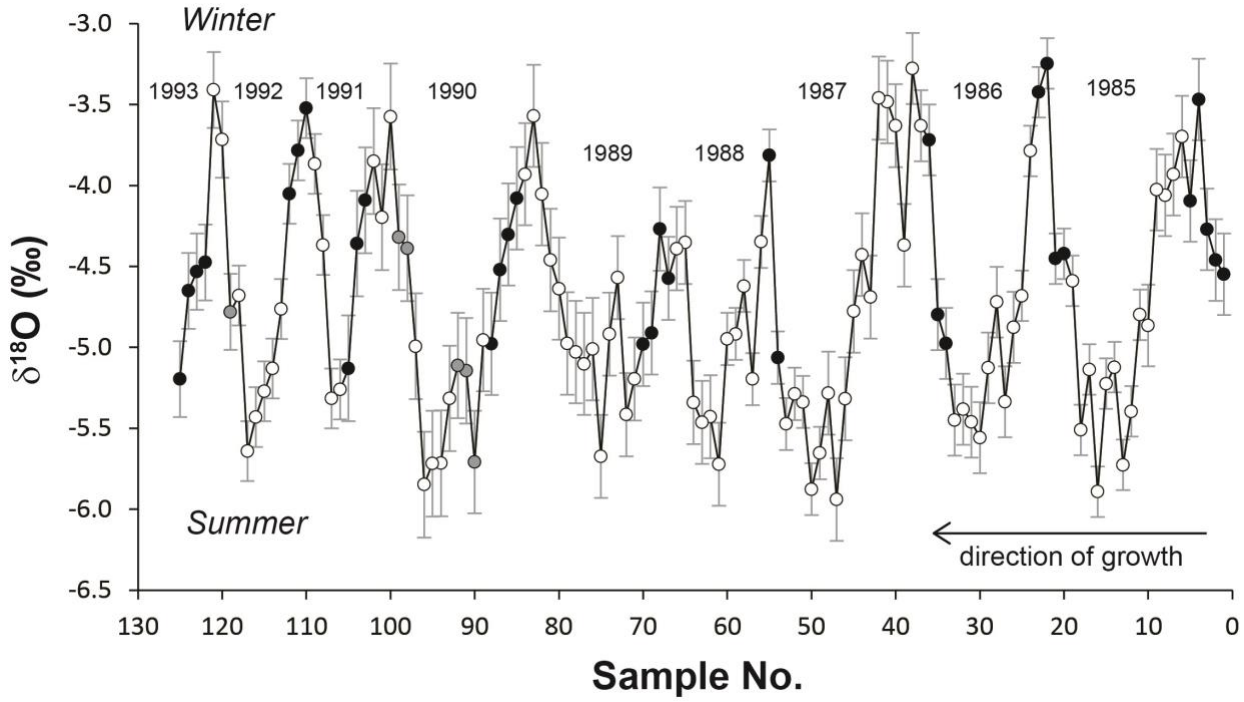

Figure 4. SIMS $\delta^{18}O$ time series in sample RFP3S-59 illustrating nine cycles labeled 1-9. Direction of growth is right-to-left on horizontal axis to match Fig. 3. Low $\delta^{18}O$ values correspond to warm temperature (summer), and higher values correspond to cooler temperature (winter). Growth direction is from right to left. White circles are location of light increments. Black circles are location of dark growth increments. Gray circles in last four cycles on the left represent ambiguous increments. Error bars = 2σ. Growth direction is from right to left.

643

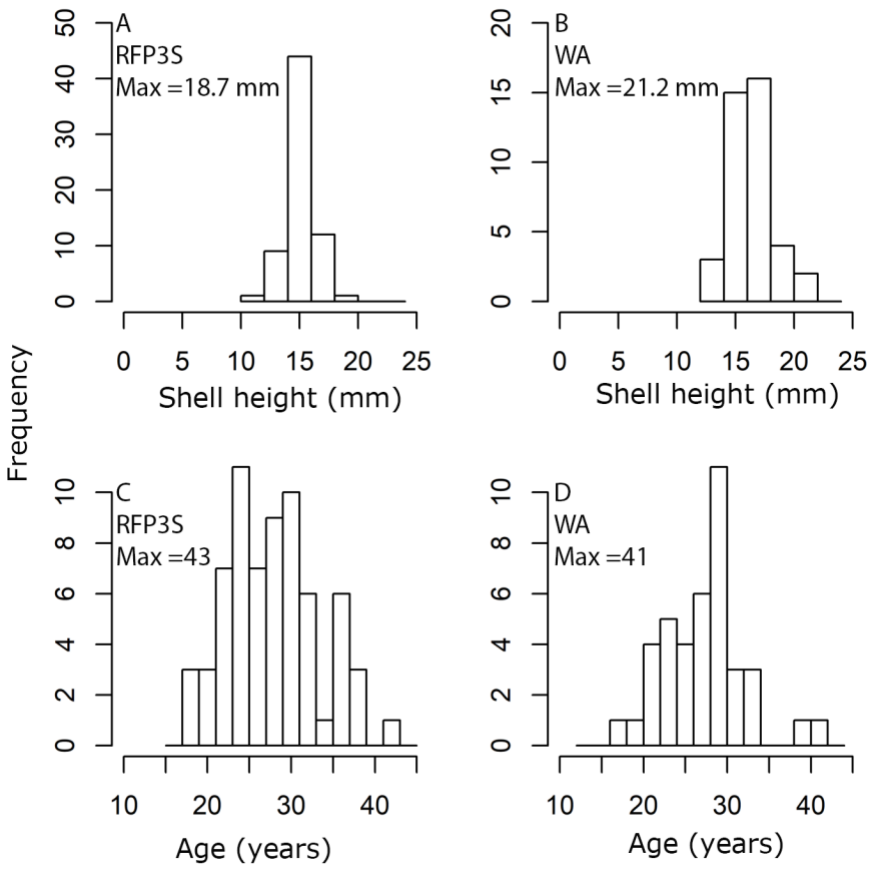

644

645 Figure 5. Histograms (counts) of shell heights and lifespans of individuals from RFP3S (n=67;

646 panels A, C) and WA (n=40; panels B, D) populations.

647

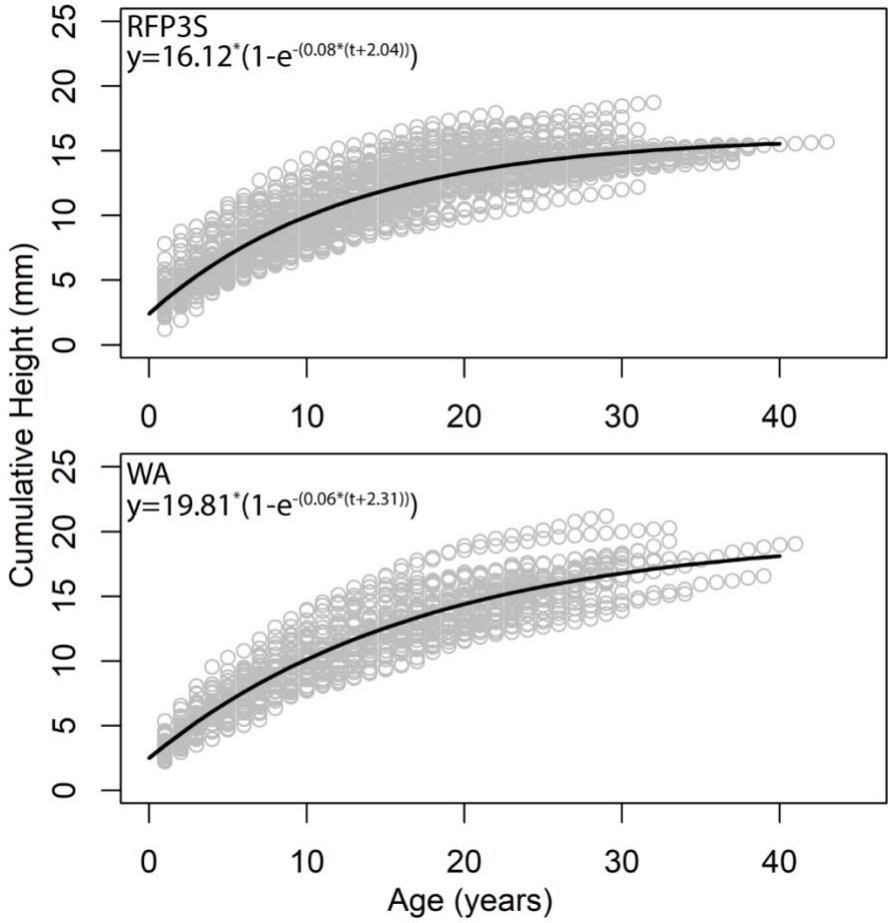

Figure 6. von Bertalanffy growth equation fit to pooled age-at-size data for both populations investigated from the Baltic Sea. Black lines represent best fit VBG equations. Grey open circles represent cumulative size-at-age for each individual (RFP3S, n=67; WA, n=40) measured.